Research Article | Vol. 28, No. 2 / 20 January 2020 / Optics Express 1369
Optics EXPRESS

Towards high power longwave mid-IR frequency combs: power scalability of high repetition-rate difference-frequency generation

QIAN CAO,[1,2] FRANZ X. KÄRTNER,[1,2] AND GUOQING CHANG[3,*]

[1]Center for Free-Electron Laser Science, DESY, Notkestrasse 85, 22607 Hamburg, Germany
[2]Department of Physics, Universität Hamburg, Luruper Chaussee 149, 22761 Hamburg, Germany
[3]Beijing National Laboratory for Condensed Matter Physics, Institute of Physics, Chinese Academy of Sciences, Beijing 100190, China
*guoqing.chang@iphy.ac.cn

Abstract: Frequency combs in the mid-IR wavelength are usually implemented by difference-frequency generation (DFG) that mixes pump pulses and signal pulses. Different from most optical parametric amplifiers that operate at a typical low repetition rate of <0.1 MHz, mid-IR frequency combs require that pump/signal pulse repetition rate must be at least as high as tens of MHz (normally >30 MHz). The DFG mixing high repetition rate (HRR) pulses limits the allowed pulse energy to prevent crystal damage. In this paper, we numerically investigate HRR DFG with a focus on the energy scalability of idler pulses. We show that HRR DFG–unlike optical parametric amplifiers–may operate in the linear regime, in which the idler pulse energy scales linearly with respect to the pump/signal pulse energy. Our simulation results suggest an efficient approach to energy scaling the idler mid-IR pulses in a HRR DFG: increase the signal pulse energy to the same level as the pump pulse energy. We also show that DFG seeded by pump/signal pulses at ~2-μm range benefits from reduced group-velocity mismatch and exhibits better idler energy scalability. For example, 44.2-nJ pulses at 9.87 μm can be achieved by mixing 500-nJ, 2.0-μm pump pulses and 100-nJ, 2.508-μm signal pulses in a 2-mm-thick GaSe crystal. At the end of this paper, we show that such high-energy signal pulses can be derived from the pump pulses using a recently invented fiber-optic method. Therefore, implementation of high-power (>2 W) longwave mid-IR frequency combs is practically feasible.

1. Introduction

Ultrafast laser sources that operate in the longwave mid-infrared (mid-IR) wavelength range of 6 to 20 μm (molecular "fingerprint" region) with 10s of MHz repetition-rate have attracted much attention in recent years [1]. If both the repetition-rate f_{rep} and the carrier-envelope offset frequency f_{ceo} of an ultrafast mid-IR laser are stabilized, the resulting frequency comb provides hundreds-of-thousands of mid-IR comb lines [2]. Equipped with rapidly developing technologies such as dual-comb detection [3–6], enhancement cavities [7,8] and electro-optic sampling [9], mid-IR frequency combs in the fingerprint region have become an enabling tool for powerful spectroscopic applications.

Due to the lack of proper gain media in the "fingerprint" region, the implementation of coherent ultrafast mid-IR lasers relies heavily upon the use of parametric frequency down-conversion from mature near-infrared (NIR) sources. Among optical parametric processes, difference-frequency generation (DFG) has become the most popular means to obtain ultrafast mid-IR pulses [10–13]. In convention, for DFG process, the input with shorter center wavelength is called *pump* and the other input is called *signal*. The generated mid-IR pulse is called *idler*. Normally, a high-power

#374278 https://doi.org/10.1364/OE.28.001369
Journal © 2020 Received 31 Jul 2019; revised 27 Nov 2019; accepted 1 Dec 2019; published 9 Jan 2020

Optics EXPRESS

near-IR laser provides the pump pulses whose center wavelength is fixed, and the signal pulses are derived from the pump pulses using nonlinear optical methods [10–14]. In this scenario, the pump pulses and the signal pulses are tightly synchronized in the time domain. Ideally, the signal pulse is wavelength tunable so that the resulting mid-IR idler can be tuned between 6–20 μm [11–13]. Moreover, if the signal pulses are derived in such a way that they share the same f_{ceo} with the pump pulses, the generated idler pulses have the f_{ceo} automatically set at zero [15], which significantly simplifies the implementation of mid-IR frequency combs [13].

Currently, mid-IR frequency combs in the "fingerprint" region (especially for wavelengths beyond 10 μm) suffer from low available average power, which leads to a reduced signal-to-noise ratio (SNR) for detection and, therefore, severely limits their use in practical spectroscopic applications. Many research efforts are geared towards finding an efficient power scaling method to achieve high-power mid-IR frequency combs [16–18].

DFG has been thoroughly investigated in the context of optical parametrical amplifier (OPA)–a device that aims to efficiently amplify the weak signal pulses by strong pump pulses. In an OPA, a weak signal pulse with a pulse energy of 10 pico-joules is amplified by a strong pump pulse, whose pulse energy normally exceeds 1 milli-joule [19]. Normally the pump is strong enough such that the amplified signal scales exponentially with respect to the pump energy–a characteristic feature that defines a practical OPA. In the following, we refer to this regime as the OPA regime. Although OPA aims to amplify signal pulses, it also produces idler pulses whose energy scales linearly (exponentially) with respect to the signal (pump) energy. Apparently for DFG operating in the OPA regime, increasing the pump energy (rather than increasing the signal energy) constitutes a more efficient method of energy scaling the idler. This operation regime seems particularly attractive because the signal pulses are usually derived from the pump pulses via inefficient nonlinear wavelength conversion such that signal pulses have 2–3 orders of magnitude less pulse energy than the pump pulses [11].

However, it is noteworthy that most OPAs have a repetition rate of <0.1 MHz; in contrast, frequency combs operate at much higher repetition rate, at least ≥30 MHz. For high repetition-rate (HRR) DFG systems, crystal damage becomes a crucial limiting factor for generating high-power mid-IR frequency combs. Moreover, due to intrinsic multi-phonon absorption, standard oxide crystals have a transparency range up to ~5 μm. To access longwave mid-IR, non-oxide crystals such as GaSe [11,13,20–25], GaAs [12], $AgGaS_2$ [26], $AgGaSe_2$ (AGSe) [20,27–29] and $ZnGeP_2$ [30,31] have been employed. Among these crystals, GaSe is one of the best candidates as it offers high nonlinearity (d_{22} = 54 pm/V), a transparent range from 0.7 to 18 μm, and sufficient birefringence for phase matching broadband inputs. Nevertheless, GaSe exhibits a lower damage threshold compared with oxide crystals that work in the near-IR wavelength range. At high pump intensity, multi-photon absorption together with poor thermal conductivity causes the temperature rising inside the crystals. When the repetition rate is as high as tens of MHz, lack of sufficient time for heat dissipation drives the crystal temperature continuously rising and eventually results in crystal breakdown. The damage threshold depends on many laser parameters (center wavelength, pulse duration, peak power, repetition rate etc.) and is normally determined experimentally. Our experimental results showed that at 30 MHz repetition rate, around 200 nJ, 200 fs pulses at 1.03 μm can damage a GaSe crystal even for a loosely focused beam radius of 200 μm [14]. This thus sets an upper limit for the total input power at 6-W, leading to a low pulse energy (and low average power) for the mid-IR output pulses.

Above analysis naturally leads to the following questions for constructing high-power mid-IR frequency combs: (1) For HRR DFG, how does the idler power scale with respect to input pump/signal power? (2) For our current experimental condition, how far are we from the OPA regime? (3) In general, how to achieve powerful HRR mid-IR pulses? In this paper we answer these questions by analyzing DFG processes inside GaSe crystals. Analytical analysis of DFG seeded with continuous waves (CWs) allows us to identify a linear operation regime, in which

Optics EXPRESS

the idler scales linearly with both the pump and the signal. Therefore increasing the signal energy is as efficient as increasing the pump energy for idler energy scaling. We then numerically investigate the DFG seeded with femtosecond pulses and show that group-velocity mismatch (GVM) plays an essential role in determining the idler energy scalability. More specifically we compare two possible DFG options for generating mid-IR pulses centered at 9.87 μm: (1) pump/signal at 1.03/1.15 μm and (2) pump/signal at 2.0/2.508 μm. We refer to them as 1-μm and 2-μm driven DFG, respectively. The GVM in the 2-μm driven DFG is much less than the 1-μm driven case, and thus exhibits superior energy scalability for the idler pulses. For example, our simulation indicates that 44.2-nJ pulses at 9.87 μm can be achieved by mixing 500-nJ, 2.0-μm pump pulses and 100-nJ, 2.508-μm signal pulses in a 2-mm-thick GaSe crystal. At 50-MHz repetition rate, this corresponds to more than 2 watts average power at the output. The key for energy scaling idler pulses in HRR DFG is to increase the signal pulse energy to the same level as the pump pulse energy. At the end of this paper, we show that such high-energy signal pulses can be derived from pump pulses using a recently invented fiber-optic method. Consequently implementation of high-power mid-IR frequency combs is practically feasible.

2. Coupled wave equations: CW case

To gain physical insight, we first revisit CW DFG process modeled by the classic coupled wave equations [32],

$$\begin{aligned}\frac{\mathrm{d}A_1(z)}{\mathrm{d}z} &= i\frac{\omega_1}{n_1 c}d_{\mathrm{eff}}A_3(z)A_2^*(z)\mathrm{e}^{-i\Delta kz},\\ \frac{\mathrm{d}A_2(z)}{\mathrm{d}z} &= i\frac{\omega_2}{n_2 c}d_{\mathrm{eff}}A_3(z)A_1^*(z)\mathrm{e}^{-i\Delta kz},\\ \frac{\mathrm{d}A_3(z)}{\mathrm{d}z} &= i\frac{\omega_3}{n_3 c}d_{\mathrm{eff}}A_1(z)A_2(z)\mathrm{e}^{+i\Delta kz},\end{aligned} \tag{1}$$

where $A_i(z)$ stands for the complex field amplitude in the longitudinal coordinate z of the nonlinear $\chi^{(2)}$ medium. The optical irradiance (intensity) $I_i(z)$ is related to the complex field amplitude by $|A_i| = \sqrt{\frac{2I_i}{\varepsilon_0 n_i c}}$, where ϵ_0 is the vacuum permittivity, c is the speed of light and n_i denotes for the refractive index of the given nonlinear medium. In the equations, ω_i is the angular frequency of the optical waves, d_{eff} the effective nonlinear coefficient, and $\Delta k = k_3 - k_2 - k_1$ the difference between the propagation wave vectors of the optical waves. Under such definition, DFG process corresponds to $\omega_1 = \omega_3 - \omega_2$. Here, we assume perfect phase matching condition $\Delta k = 0$.

The exact solution to Eq. (1) can be written in the mathematical form of Jacobi elliptic functions [32,33]. When the idler wave has zero input and the pump is undepleted, the output idler can be expressed as

$$\begin{aligned}I_1(z) &= \frac{\omega_3}{\omega_2}I_{20}\sinh^2(\Gamma z),\\ \Gamma^2 &= \frac{2\omega_2\omega_1 d_{\mathrm{eff}}^2}{n_1 n_2 n_3 \varepsilon_0 c^3}I_{30}.\end{aligned} \tag{2}$$

Here I_{i0} is the intensity at the input.

To investigate DFG at different launching conditions, we consider type-I DFG inside a 0.2-mm-thick GaSe crystal. The e-polarized pump is set at 1030 nm and the o-polarized signal at 1150 nm. The generated o-polarized idler is then at 9.87 μm. The input signal has a fixed intensity of 20 MW/cm^2 and the input pump intensity varies from 10 MW/cm^2 to 10^3 GW/cm^2. The pump, signal, and idler at the crystal output are calculated using the exact analytic solution. The sinh square expression is also used for calculating the idler as a comparison. Figure 1(a) illustrates the output intensity of the three waves as a function of input pump intensity. The total intensity of the input waves is also plotted as a dashed-dotted line. As Fig. 1(a) shows, the idler (black

Optics EXPRESS

solid line) experiences three different stages as the pump increases. For the pump intensity below 10 GW/cm^2, the idler grows linearly with respect to the pump. We refer to this DFG operation regime as the linear regime. When the pump intensity falls between 10–200 GW/cm^2, the idler grows exponentially, corresponding to the OPA regime for the DFG process. When the pump intensity exceeds 200 GW/cm^2, the idler growth starts to saturate and reaches a maximum for the pump intensity at about 300 GW/cm^2. At the maximum, DFG process converts all the pump photons into the signal/idler photons and the pump is completely depleted. After that, the back conversion process occurs and the signal/idler photons are back-converted to the pump.

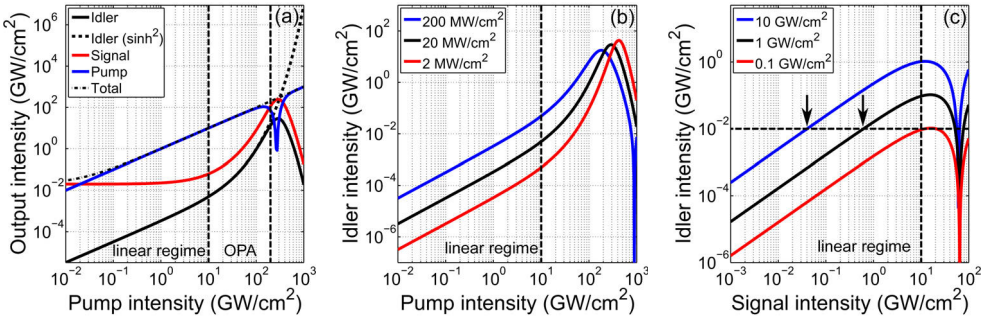

Fig. 1. DFG outputs under different launching conditions. (a) DFG outputs when the signal is fixed at 20 MW/cm^2. The idler growth has three different stages. When the pump is below 10 GW/cm^2, the idler has a linear growth. (b) DFG process with a fixed signal at three different levels. The idler grows linearly as the pump is below the threshold level. (c) DFG process with a fixed pump. The idler grows linearly as the signal is below the saturation level.

Within the linear regime and the OPA regime, the idler calculated by the exact solution (black solid line) and the sinh square expression (black dashed line) are identical. Thus we can use the latter expression to write the idler in a more analytical fashion. In Eq. (2), the unitless parameter Γz represents the strength of the parametric interaction, which determines the operation regime for the DFG process. When $\Gamma z \ll 1$, the parametric interaction is weak and the DFG process operates in the linear regime. We can write the sinh square function using its first order Taylor expansion, which leads to

$$I_{\text{idler}} = \frac{2\omega_1\omega_3 d_{\text{eff}}^2}{n_1 n_2 n_3 \varepsilon_0 c^3} \cdot I_{20} \cdot I_{30} \cdot L^2. \tag{3}$$

Here L is the crystal thickness. This expression clearly shows that for DFG in the linear regime, the output idler intensity is proportional to the product between the input pump intensity and the input signal intensity, and therefore increasing the signal has the same effect as increasing the pump for scaling up the idler. In contrast, the OPA regime corresponds to the case when $\Gamma z \gg 1$; the sinh function can be approximated by the exponential function, and the idler is written as

$$I_{\text{idler}} = \frac{1}{4} \cdot \frac{\omega_3}{\omega_2} \cdot I_{20} \cdot e^{2\Gamma z}. \tag{4}$$

Equation (4) shows that the output idler scales exponentially with respect to the square root of the input pump and linearly to the input signal. Therefore in the OPA regime, increasing the pump is more efficient for scaling up the idler compared with increasing the signal.

We can define a threshold pump intensity I_{th} that separates the linear regime and the OPA regime by setting Γz unity. I_{th} is written as

$$I_{\text{th}} = \frac{n_1 n_2 n_3 \varepsilon_0 c^3}{2\omega_1\omega_2 d_{\text{eff}}^2} \cdot (\frac{1}{L})^2. \tag{5}$$

Optics EXPRESS

For our DFG calculation (0.2-mm-thick GaSe, type-I DFG process with 1030 nm and 1150 nm inputs), the threshold pump intensity is 7.3 GW/cm^2 according to this expression, which is close to the results shown in Fig. 1(a).

To show specifically how the idler scales in different operation regimes, we set the input signal at 2 MW/cm^2, 20 MW/cm^2 and 200 MW/cm^2, respectively, and then calculate the idler as a function of the pump using the exact solution. The results in Fig. 1(b) show that, for all three DFG processes, the idler grows linearly until the input pump reaches a threshold intensity of around 10 GW/cm^2. It is consistent with the theoretical prediction from Eq. (2), as the parametric gain Γz is independent on the level of the signal intensity. It is also noteworthy that DFG processes seeded with different input signal saturate at different pump intensities. After saturation, the signal/idler photons are back-converted to the pump photons.

To inspect how the idler scales with respect to the signal, we calculate the DFG process with the input pump fixed at 0.1 GW/cm^2, 1 GW/cm^2 and 10 GW/cm^2 while the input signal increases from 1 MW/cm^2 to 100 GW/cm^2. The idler is again calculated by the exact solution and the results are plotted in Fig. 1(c). For all three traces, the DFG process stays in the linear regime when the input signal is below 10 GW/cm^2, regardless of the input pump intensity. When the signal exceeds 10 GW/cm^2, the idler growth starts to saturate and then reaches a maximum. After that, the idler drops as it is back-converted into the pump and then rises again. The saturation intensity for the signal is close to the threshold intensity for the pump I_{th}. In the theory of optical parametric interactions [33], the parametric gain coefficient Γ is actually related with the total input intensity $I_{20} + I_{30}$ (more precisely, the total photon flux of the inputs). Therefore as long as the input intensity is below a certain threshold value, the parametric interaction is weak and the DFG process stays in the linear regime.

Figure 1(c) also suggests the advantage of scaling up the idler by increasing the signal. For example, the two marked points in Fig. 1(c) correspond to the DFG processes that generate the same amount of idler. However, the point on the black trace corresponds to a total pump-signal input intensity of ~1.6 GW/cm^2, while the other one on the red trace has a total input intensity of ~10 GW/cm^2. Indeed Eq. (3) clearly indicates that for producing the same amount of idler, setting the input signal intensity equal to the input pump intensity can minimize the total optical intensity incident onto the crystal. It corresponds to a DFG process with higher photon conversion efficiency and less thermal load to the crystal.

3. Towards high-power HRR mid-IR femtosecond sources

Implementation of mid-IR frequency combs via DFG involves mixing of femtosecond pulses. Nevertheless, above analysis of the CW case provides physics insight on the energy scaling property of an HRR mid-IR DFG source. The essential difference between the CW case and the pulsed case is that the field amplitude in the pulsed case now becomes time dependent to describe a pulse envelope. In general, DFG process involving femtosecond pulses can be modeled as

$$\begin{aligned}
\frac{\partial A_1(z,\tau)}{\partial z} + \left(\frac{1}{v_{g,1}} - \frac{1}{v_{g,3}}\right)\frac{\partial A_1(z,\tau)}{\partial \tau} + \frac{i\beta_{2,1}}{2}\frac{\partial^2 A_1(z,\tau)}{\partial \tau^2} &= i\frac{\omega_1 d_{\text{eff}}}{n_1 c} A_3 A_2^* e^{-i\Delta k z}, \\
\frac{\partial A_2(z,\tau)}{\partial z} + \left(\frac{1}{v_{g,2}} - \frac{1}{v_{g,3}}\right)\frac{\partial A_2(z,\tau)}{\partial \tau} + \frac{i\beta_{2,2}}{2}\frac{\partial^2 A_2(z,\tau)}{\partial \tau^2} &= i\frac{\omega_2 d_{\text{eff}}}{n_2 c} A_3 A_1^* e^{-i\Delta k z}, \\
\frac{\partial A_3(z,\tau)}{\partial z} + \frac{i\beta_{2,3}}{2}\frac{\partial^2 A_3(z,\tau)}{\partial \tau^2} &= i\frac{\omega_3 d_{\text{eff}}}{n_3 c} A_1 A_2 e^{+i\Delta k z}.
\end{aligned} \tag{6}$$

Here the retarded time τ is introduced with $\tau = t - \frac{z}{v_{g,3}}$. $v_{g,i} = \partial\omega_i/\partial k_i$ and $\beta_{2,i}$ denote the group velocity and group velocity dispersion (GVD) of each pulse, respectively. Both GVM and GVD

Optics EXPRESS

are strongly wavelength dependent, and therefore we will discuss HRR DFG pumped at two different wavelengths: 1.03 μm versus 2 μm.

3.1. 1-μm driven HRR DFG

We first simulate type-I DFG process inside a 2-mm-thick GaSe crystal. At the input, the pump is a 170-fs, 100-nJ sech^2 pulse at 1030 nm and the signal is a 130-fs, 1-nJ sech^2 pulse at 1150 nm; the idler pulse centered at 9.87 μm is set as zero. Both the pump and the signal beams are focused at the center of the crystal with a beam size of 200 μm in radius. Due to group-velocity mismatch (GVM), propagation through 2-mm GaSe generates 193-fs pump/signal walk-off. At the input, we place the pump pulse ahead of the signal pulse by 96.5 fs, one half of the total walk-off. Because the signal pulse travels faster than the pump pulse ($v_{g,2} = c/2.912$ versus $v_{g,3} = c/2.941$), the signal pulse passes through the pump pulse and stays 96.5 fs ahead of the pump at the crystal output. In this scenario, the pump-signal temporal overlapping is nearly maximized, which guarantees efficient generation of the idler pulse.

We use the standard split-step Fourier method to solve the coupled wave equations for optical pulses. The normalized intensity profiles of the outputs are plotted in Fig. 2(a). The signal pulse at the input (red dashed line) is also plotted for illustrating the temporal walk-off. In the figure, the idler pulse is magnified by 5,000 and the signal pulses by 50 for better visibility. The inset plots the idler spectrum at the output. The idler pulse travels fastest inside the GaSe crystal with a group velocity of $v_{g,1} = c/2.761$. Consequently, the newly generated idler quickly moves out of the pump-signal overlapping region and therefore the idler pulse at the output has a FWHM duration of 800 fs, much longer than the pump/signal pulses. At the crystal output, the idler pulse energy is 15.1 pJ (We already consider the Fresnel reflection losses at both crystal facets), corresponding to 0.45-mW average power for 30-MHz repetition rate.

In the spectral domain, the idler has a spectral bandwidth of 260 nm, which supports a 420-fs transform-limited (TL) pulse. Adding a negative group-delay dispersion (GDD) of -43,000 fs^2 can compress the idler pulse to 525 fs with a peak intensity about 85% of the TL pulse. Figure 2(b) plots the normalized intensity profiles of the output pulse (black line), the compressed pulse (blue line) and the TL pulse (red line). The instantaneous frequency of the idler pulse before compression (black dashed line in Fig. 2(b)) shows that the uncompressed idler is negatively chirped in the leading part and positively chirped in the trailing part. Such a chirping profile is due to the complicated interaction of GVM and GVD, and consequently, the idler pulse can be compressed using either positive GDD or negative GDD. We screen the dechirping GDD and calculate the peak intensity of the compressed idler pulse. Figure 2(c) plots the relative peak intensity of the compressed pulse versus the compressing GDD. For GDD at -43,000 fs^2 and +41,500 fs^2, the compressed pulse (blue line in the inset of Fig. 2(c)) reaches a peak intensity of 85% and 82% of the TL pulse (red dashed line in the inset of Fig. 2(c)).

To investigate the power scaling, we simulate the DFG processes by setting the input signal energy at 0.1 nJ, 1 nJ, and 10 nJ. For each signal energy we increase the input pump energy from 0.1 nJ to 4 μJ. Other parameters remain unchanged. Figure 3(a) shows the pulse energy of the output idler as a function of input pump-pulse energy. As we expect from the CW case, DFG in the pulsed case can operate in the linear regime or the OPA regime as well. For the pump energy below 300 nJ, the idler pulse energy at the GaSe output scales linearly with respect to the input pump energy even as the input signal energy varies from 0.1 nJ to 10 nJ. When the pump exceeds 300 nJ, the DFG process transits into the OPA regime in which the output idler grows exponentially as a function of the input pump energy.

At low repetition rate (≤0.1 MHz), input pump pulses with μJ–mJ pulse energy are allowed [19] for seeding the DFG process, making DFG operate in the OPA regime. For HRR (e.g., ≥30 MHz) DFG systems, crystal damage limits the allowed input pulse energy at the hundreds of nJ level such that DFG can only operate in the linear regime. It is noteworthy that, when plotting

Optics EXPRESS

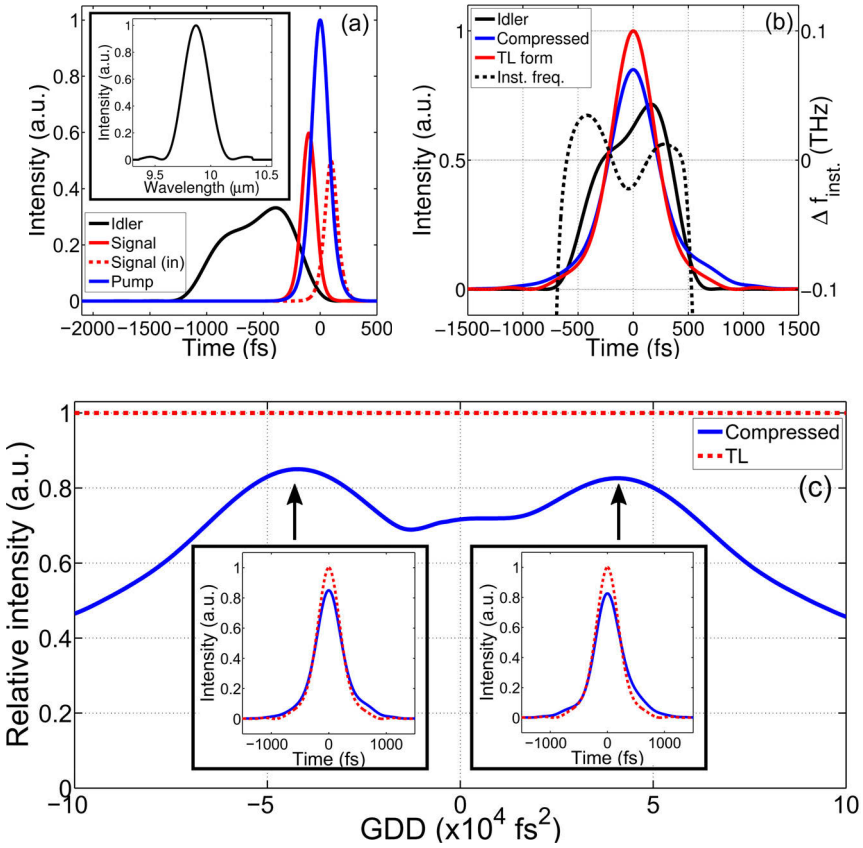

Fig. 2. DFG process inside 2-mm-thick GaSe. (a) Pulse profile at the output. The input signal pulse is also plotted. The signal in the graph is magnified by a factor of 50 and the idler by 5,000. Inset: output idler spectrum. (b) Output idler pulse before compression, after compression, and its TL form. The dashed curve shows the instantaneous frequency. (c) Peak intensity of the dechirped pulse against dechirping GDD. Inset: compressed pulse profile (blue curve) and TL pulse profile (red dashed curve).

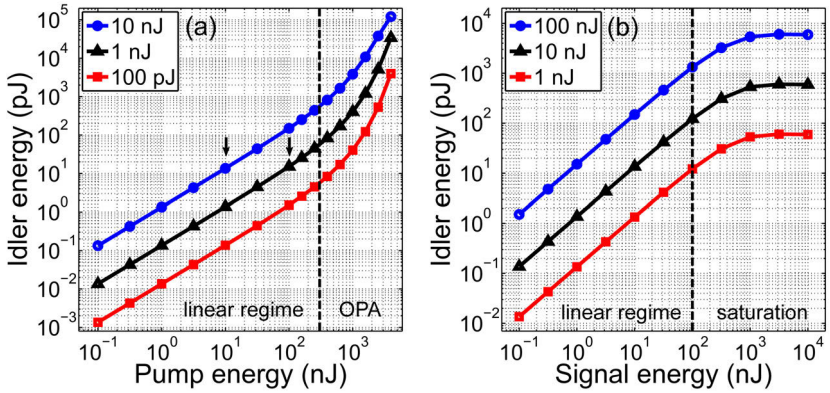

Fig. 3. Scaling of idler pulse energy under different input conditions. (a) Scaling of idler energy versus input pump energy given input signal energy fixed at 100 pJ, 1 nJ, and 10 nJ. GaSe thickness: 2 mm. (b) Scaling of idler energy versus input pump energy given input signal energy fixed at 1 nJ, 10 nJ, and 100 nJ. GaSe thickness: 2 mm.

Optics EXPRESS

the simulation results for the pulsed case, we use the pulse energy rather than the optical intensity to better quantify the three pulses. We can also translate pulse energy into corresponding peak intensity to compare with the CW case. For example, the pump threshold of 300 nJ with 200-μm beam waist and 170-fs pulse duration corresponds to a peak intensity of 1.4 GW/cm^2. For the CW case to have a pump threshold intensity at 1.4 GW/cm^2, the required GaSe thickness needs to be only 0.46 mm according to Eq. (5), which is much shorter than 2 mm—the GaSe thickness for the pulsed case. This is apparently anticipated because the GVM-caused walk-off weakens the interaction between the pulses, leading to an effective interaction length shorter than the actual thickness of the crystal.

The three curves in Fig. 3(a) also suggest that different combinations of pump-signal energy can generate idler with the same pulse energy. For example, DFG between 10-nJ pump and 10-nJ signal results in 15-pJ idler pulses (marked by arrow at point); the same idler pulse energy can also be achieved using 100-nJ pump and 1-nJ signal (the marked triangle point). Given that a higher pulse energy may damage the crystal, the former scheme (i.e., 10-nJ pump and 10-nJ signal) is preferred. Furthermore, this scheme has an improved efficiency of converting near-IR photons to mid-IR photons.

To show how the idler pulse energy scales with the signal pulse energy, we calculate the DFG processes with the pump energy fixed at 1 nJ, 10 nJ and 100 nJ and the signal energy increased from 0.1 nJ to 10 μJ. As the results in Fig. 3(b) show, the idler pulse energy grows linearly until the input signal reaches about 100 nJ, and then the idler growth starts to saturate. Different from the CW case (Fig. 1(c)), the large temporal walk-off of the idler pulse from the pump/signal pulses prevents back conversion such that the idler pulse energy eventually saturates to a constant value. Nevertheless DFG between 100-nJ pump and 100-nJ signal in a 2-mm-thick GaSe generates idler pulse of about 1.3-nJ energy, corresponding to about 40-mW average power for a 30-MHz laser system. At 30-MHz repetition rate, the pulse energy at the input is still below the crystal damage threshold according to our previous experimental results [14].

The results in Figs. 3(a) and 3(b) indicate that the idler pulse energy scales linearly with the pulse-energy product between the pump pulse and the signal pulse when the DFG process operates in the linear regime. Therefore, increasing the pump energy or the signal energy leads to the same scaling of the idler energy.

To further show the effect of crystal thickness, we simulate the DFG process with the GaSe thickness varying from 0.5 mm to 4 mm. The input energies of the pump and signal are both set at 100 nJ. Other parameters remain the same as previous. The results in Fig. 4(a) show that the output idler pulse becomes longer for a thicker crystal due to a larger temporal walk-off effect. Figure 4(b) plots the idler pulse energy as a function of GaSe thickness, showing that the idler energy starts to saturate as the crystal thickness exceeds 3 mm. Nevertheless 1.5-nJ idler pulses can be generated using a 3-mm thick GaSe crystal, which corresponds to a pump-to-idler quantum efficiency of 25%.

In addition, crystal thickness affects the idler pulse's spectral bandwidth due to the phase matching condition. The black dashed curve in Fig. 4(c) plots the spectral bandwidth of the idler versus the crystal thickness. The idler bandwidth decreases from 770 nm to 140 nm as the GaSe thickness increases from 0.5 mm to 4 mm. We plot in the same figure the FWHM duration of the idler pulse (circle), the compressed pulse (triangle) by adding a dechirping GDD to the idler spectrum, and the corresponding TL pulse (square). The uncompressed idler pulse has a duration varying from 300 fs to 1180 fs. For a thinner crystal ($\leq$1 mm), the output idler pulse is nearly transform-limited; for a thicker crystal, the temporal walk-off renders a complicated chirp to the idler pulse and degrades the quality of the compressed pulses.

For certain nonlinear applications in the mid-IR wavelength range (e.g., supercontinuum generation and high harmonic generation), pulse peak power is of particular importance. Figure 4(d) shows the peak power as a function of GaSe thickness for the output idler pulse

Optics EXPRESS

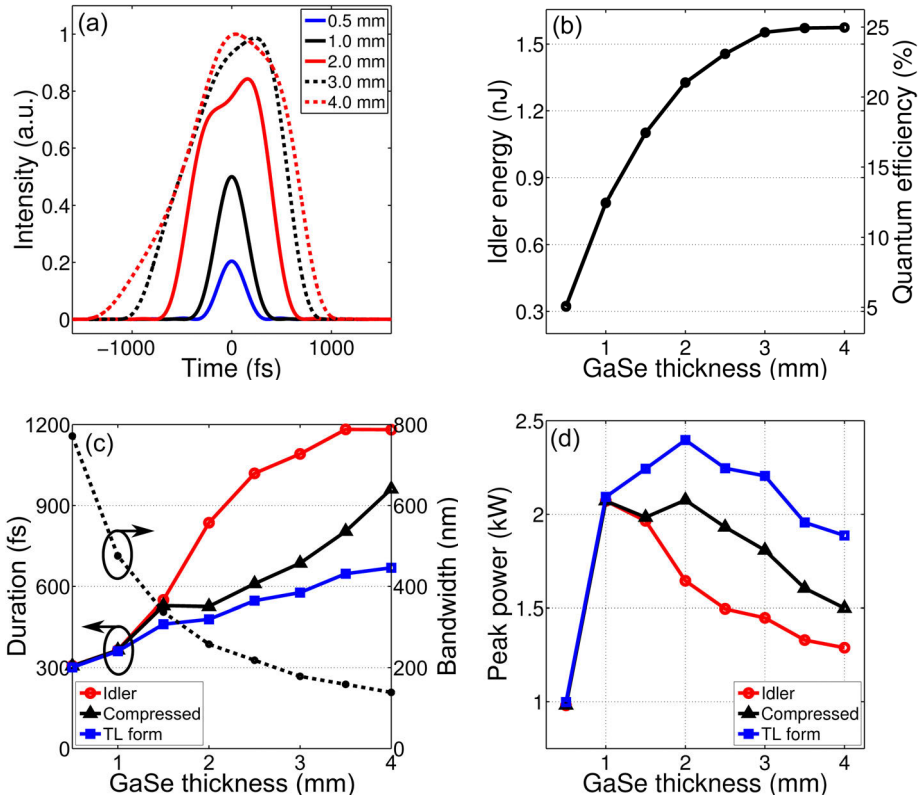

Fig. 4. Effect of GaSe thickness on idler pulse in 1-μm driven DFG. (a) Idler pulse profiles for GaSe thickness of 0.5 mm, 1.0 mm, 2.0 mm, 3.0 mm, and 4.0 mm. (b) Idler pulse energy versus crystal thickness. (c) Pulse duration of output pulse (red circle), compressed pulse (black triangle), and TL pulse (blue square) and spectral bandwidth versus GaSe thickness. (d) Peak power of output pulse (red circle), compressed pulse (black triangle), and TL pulse (blue square) versus GaSe thickness.

(circle), the compressed pulse (triangle), and the TL pulse (square). All the peak powers decrease with the increased GaSe thickness when the crystal becomes thicker than 2 mm, which causes a smaller phase matching bandwidth and a larger temporal walk-off. If higher peak power rather than higher pulse energy is preferred by the applications, the results in Fig. 4(d) suggests that a GaSe of 1 mm thick is best suited; the resulting idler pulse requires no post compression and has a peak power of 2.1 kW.

3.2. 2-μm driven HRR DFG

Above analysis shows that energy scaling the mid-IR idler in 1-μm driven HRR DFG is limited by two features related with the GaSe crystal: (1) allowed pump/signal pulse energy and (2) large GVM. GaSe has a bandgap of ~2.1 eV and exhibits strong two-photon absorption for pulses with a center wavelength shorter than ~1.18μm. When the pump/signal pulses are centered at 1.03/1.15 μm at a repetition rate of 30 MHz, the pulse energy is capped under 200 nJ to prevent catastrophic crystal damage. In addition, the associated pump-signal GVM is 95 fs/mm, leading to a weak parametric interaction among the pump, signal, and idler. The rapid walk-off among these pulses rules out the energy scaling method of increasing the crystal thickness. Even worse, the large GVM between the pump/signal with the idler may exert complicated chirp to the output

Optics EXPRESS

idler pulse, make it uncompressible, and compromise the peak power. As a result of these two disadvantageous features, the mid-IR pulse at 9.87 μm generated by 1-μm driven HRR DFG is limitd to ~1.5 nJ in pulse energy and ~2 kW in peak power (Fig. 4).

The detrimental two-photon absorption can be effectively prevented by using input pulses with longer center wavelengths. Indeed, the GVM can be reduced as well. Figure 5(a) plots pump-idler and pump-signal GVM coefficients for DFG processes with the pump centered at 1.03 μm and 2.0 μm. For both pumping wavelengths, the DFG is set to generate an idler pulse varying from 5–15 μm. Apparently the GVM becomes much smaller for DFG seeded by pump and signal pulses at ~2.0 μm. For example, the pump-idler (black solid curve) GVM is about 600 fs/mm and the pump-signal (blue solid line) GVM about 95 fs/mm for generating a 10 μm idler with the pump at 1.03 μm. For DFG using pump pulses at 2 μm, these two GVMs drop to 32 fs/mm and 16 fs/mm, which results in less temporal walk-off and enhances the parametric interaction between these three pulses. The results in Section 3.1 indicate that GVM plays a crucial role for pulsed DFG and determines how effectively the three waves can exchange energy. A straightforward speculation is that smaller GVM allows the use of thicker GaSe crystals and, therefore, significantly increases the yield of mid-IR pulse energy or reduces the amount of pump and signal power necessary to achieve a given idler-power.

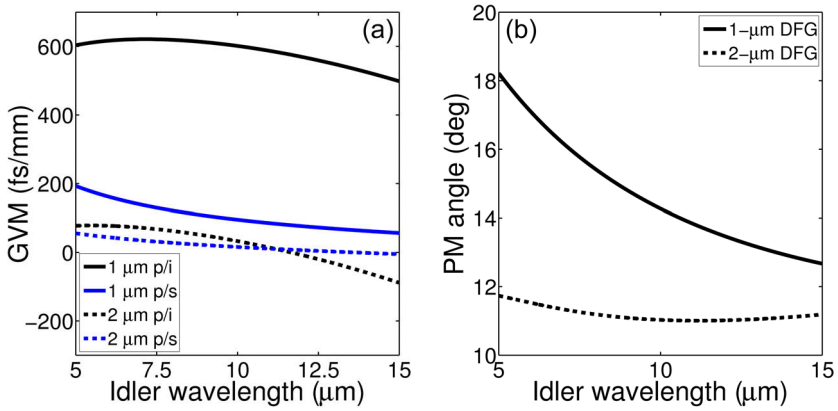

Fig. 5. Comparison between 1-μm driven DFG and 2-μm driven type-I DFG inside GaSe. (a) GVM for 1-μm pump and 2-μm pump. The temporal walk-off between the pump and the signal is about 5 time less for the case of 2-μm pump. (b) Phase matching condition for type-I DFG process inside GaSe.

Besides GVM, shifting the pump wavelength from 1.03 μm to 2 μm also changes the phase matching condition of the DFG process. Figure 5(b) plots the phase matching angle for a GaSe crystal for type-I DFG. For generating the idler pulses between 5–15 μm, the phase matching angle varies about 5 degrees for the 1-μm driven DFG; for the 2-μm driven DFG, it changes less than 1 degree. Such a small variation of the phase matching angle over wavelength corresponds to also larger acceptance angle in favor of tightly focused beams as well as a large acceptance bandwidth allowing the generation of extremely short mid-IR pulses [34].

To compare energy scalability with the 1-μm driven DFG, we simulate the 2-μm driven DFG by setting the input signal energy at 0.1 nJ, 1 nJ and 10 nJ, and for each signal energy the input pump energy varies from 0.1 nJ to 4 μJ. The GaSe thickness is set at 2 mm as well. The three curves in Fig. 6(a) exhibit similar dependence on input pump pulse energy as those curves in Fig. 3(a). However, due to lower GVM, 2-μm driven DFG exhibits a better energy scalability. For example, at the same input condition of 100-nJ pump and 10-nJ signal, the 1-μm driven DFG

Optics EXPRESS

generates idler of 0.15 nJ while the 2-μm one generates 0.98 nJ idler, representing nearly one order of magnitude improvement.

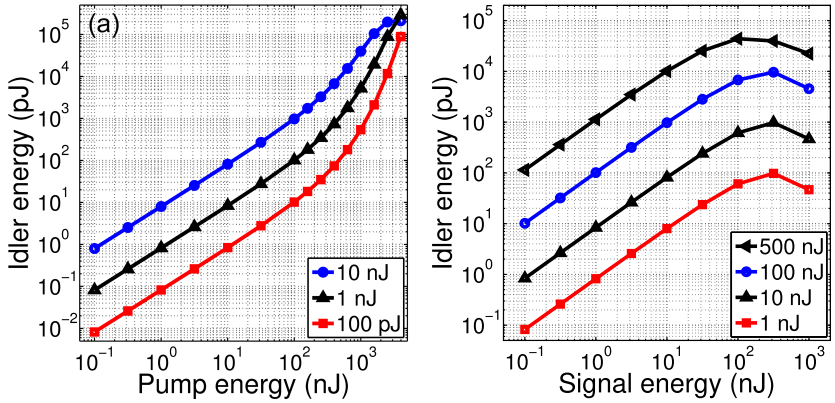

Fig. 6. Scaling of idler pulse energy under different input conditions. (a) Scaling of idler energy versus input pump energy given input signal energy fixed at 100 pJ, 1 nJ, and 10 nJ. GaSe thickness: 2 mm. (b) Scaling of idler energy versus input signal energy given input pump energy fixed at 1 nJ, 10 nJ, 100 nJ and 500 nJ. GaSe thickness: 2 mm.

To show how the idler pulse energy scales with the signal pulse energy, we calculate the DFG processes with the pump energy fixed at 1 nJ, 10 nJ and 100 nJ, and the signal energy increased from 0.1 nJ to 1 μJ; the results are shown as red square curve, black upward-pointing triangle curve and blue circle curve in Fig. 6(b). Similar as the results in Fig. 3(b), the idler pulse energy in the 2-μm driven DFG grows linearly and then starts to saturate as the input signal pulse increases. However, a distinct difference appears for the signal energy increased beyond 300 nJ: the idler energy saturates to a constant value in the 1-μm driven DFG while it drops to a lower value in the 2-μm case. This is also due to less GVM in the 2-μm DFG, which leads to a more efficient interaction of the three waves such that power back conversion from signal/idler to pump takes place when the signal energy exceeds 300 nJ.

In [23], 30-W, 32-fs pulses generated by a Tm-fiber laser at 2-μm with 50-MHz repetition rate are incident onto a GaSe crystal for intra-pulse DFG. The results indicate that 600-nJ pulse energy at 2-μm remains below the crystal damage threshold given that the peak intensity at the focus reaches 75 GW/cm^2 [23]. As the results in Fig. 6(a) show, the HRR DFG starts to enter OPA regime as the pump pulse energy exceeds 100 nJ. To show how the idler pulse energy scales with the input signal energy when the DFG operates in the OPA regime, we plot in Fig. 6(b) black left-pointing triangle curve corresponding to 500-nJ pump energy. In the OPA regime, the idler starts to saturate at a lower input signal pulse energy of 100 nJ. Nevertheless, our simulation results indicate that DFG between a 500-nJ pump pulse and 100-nJ signal pulse in a 2-mm-thick GaSe crystal generates an idler pulse with 44.2-nJ energy and 135-fs duration, corresponding to 317-kW peak power. At 50-MHz repetition rate, the average power is as high as 2.2 Watts.

To investigate the effect of crystal thickness and compare with the 1-μm driven DFG, we simulate the 2-μm DFG process with the GaSe thickness varying from 0.5 mm to 4 mm and the input energies of the pump and signal are both set at 100 nJ. Due to less GVM, the output idler pulses shown in Fig. 7(a) have a more symmetric pulse profile compared with their 1-μm counterparts as shown in Fig. 4(a). Figure 7(b) plots the pulse energy as a function of GaSe thickness, showing that the idler energy starts to saturate as the crystal thickness exceeds 3.5 mm; Using 3-mm-thick GaSe, 9.58-nJ idler pulses can be generated, representing 6 times improvement compared with the 1-μm driven DFG (1.55 nJ idler pulse energy). For a repetition rate of 30 MHz, such pulse energy leads to ~300-mW average power. Unlike the case of 1-μm driven DFG,

Optics EXPRESS

where excessive pump-signal temporal walk-off limits the use of thicker GaSe for scaling the idler, the saturation of the idler growth in the 2-μm driven DFG is due to the depletion of the pump photons. We plot in Fig. 7(b) the pump-to-idler photon conversion efficiency. For 2-μm driven DFG, the photon conversion ratio can exceed 76%, 3 times higher than the case of 1-μm driven DFG (24.5%).

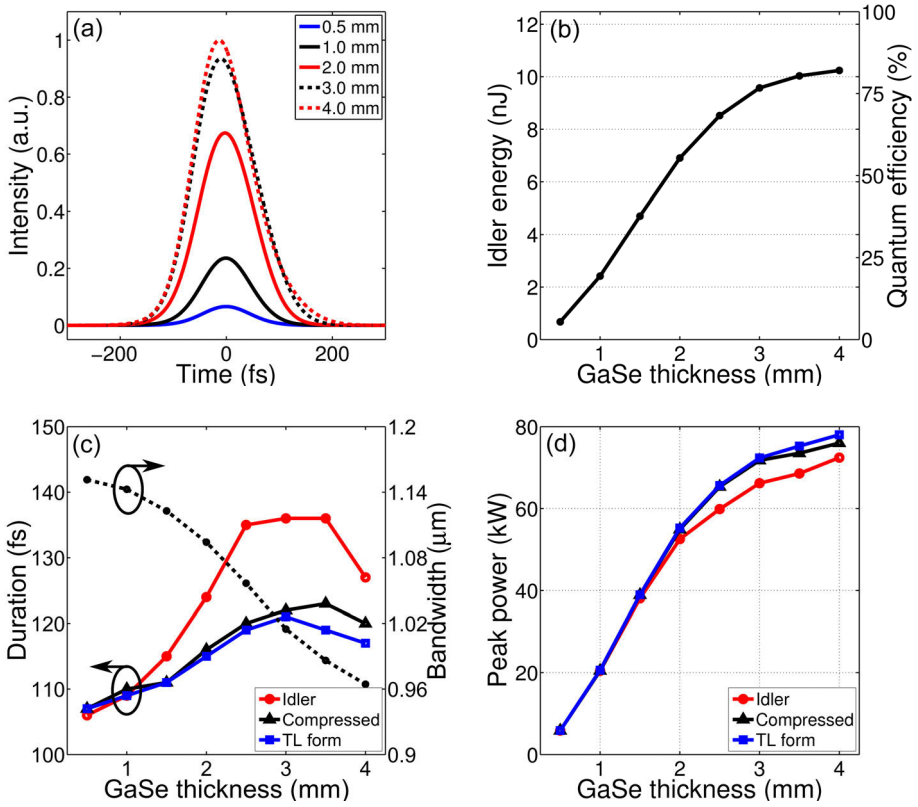

Fig. 7. Effect of GaSe thickness on idler pulse in 2-μm driven DFG. (a) Idler pulse profiles for GaSe thickness of 0.5 mm, 1.0 mm, 2.0 mm, 3.0 mm, and 4.0 mm. Inset: idler pulse energy versus crystal thickness. (b) Pulse duration of output pulse (red circle), compressed pulse (black triangle), and TL pulse (blue square) and spectral bandwidth versus GaSe thickness. (c) Peak power of output pulse (red circle), compressed pulse (black triangle), and TL (blue square) versus GaSe thickness.

Figure 7(c) plots the spectral bandwidth versus the crystal thickness (black dashed line, to the right axis). The idler bandwidth decreases from 1150 nm to 964 nm as the crystal thickness increased from 0.5 mm to 4 mm. Clearly the idler resulted from 2-μm driven DFG has a much larger spectral bandwidth than can be achieved from the 1-μm driven DFG. Consequently the idler pulse generated from 2-μm driven DFG is much shorter with the duration varying between 105 fs and 135 fs (circle marked line in Fig. 7(c)). Given that the corresponding TL pulse duration varies between 105 fs and 120 fs (square marked line in Fig. 7(c)), the idler pulse is close (within 85%) to be transform-limited. By simply adding proper GDD, the idler pulse can be dechirped to be nearly transform-limited (triangle marked line in Fig. 7(c)).

Figure 7(d) shows the peak power as a function of GaSe thickness for the output idler pulse (circle), the compressed pulse (triangle), and the TL pulse (square). Different from the 1-μm driven DFG, peak powers in the 2-μm case increase accordingly with the increased GaSe. Thanks

Optics EXPRESS

to the short pulse duration and higher pulse energy, the idler peak power can reach as high as 72 kW when 4-mm GaSe is used for 2-μm driven DFG, nearly two orders of magnitude improvement from the 1-μm case (1.3 kW). Such a high peak power is crucial for important nonlinear mid-IR applications.

4. Possible experimental implementation

In DFG, the signal pulses are usually derived from the pump pulses using second-order nonlinear susceptibility offered by nonlinear optical crystals or third-order nonlinearity in an optical fiber. The latter method is more attractive as the derived signal pulses share the same f_{ceo} as the pump pulses and the resulting mid-IR pulses have set f_{ceo} automatically to zero. To convert the resulting mid-IR sources into mid-IR frequency combs, only the repetition rate f_{rep} needs to be stabilized, which significantly simplifies the overall experimental setup. In general, however, optical fibers exhibit poor energy scalability due to the massive amount of nonlinearity caused by the tight confinement of the femtosecond pulses in a small mode area. As a result, the signal pulses that are derived using fiber-optic methods are normally much weaker than the pump pulses. For example, a widely used fiber-optic method to obtain the signal pulses is to employ Raman soliton self-frequency shifting in an optical fiber [11]. Raman soliton pulses normally have nanojoule or even sub-nanojoule level pulse energy, especially for the case where the pump pulses are centered at 1.03 μm, an operating wavelength range for mature high-power Yb-doped fiber laser systems. For example, Ruehl *et al.* used a 2.2-W, 151-MHz Yb:fiber laser source to derive the signal pulses by generating Raman solitons in 25-cm-long highly nonlinear suspended-core fiber [11]. The resulting signal pulses are tunable between 1.15 to 1.65 μm with pulse energies varying from 0.04–0.15 nJ. After mixing the signal and the pump in a 0.5-mm-thick GaSe crystal, the DFG process produces 0.3-mW average output power at 10 μm, which corresponding to 2-pJ pulse energy in the mid-IR range. For 2-μm driven inter-pulse DFG, Phillips *et al.* used a 72-MHz Tm-fiber laser system that produces 150-fs, 2.0-μm pulses with watt-level average power [12]. The signal pulses obtained via Raman soliton generation in fluoride fiber centers at 2.5-μm with 30-mW average power, corresponding to a pulse energy of 0.42-nJ. Using a quasi-phase-matching DFG scheme in 2-mm-thick orientation-patterned GaAs, they generated 6.7–12.7-μm idler pulses with 1.3-mW average power.

The simulation results presented in Section 3 clearly point towards a more efficient way for power scaling of HRR DFG: increase the signal pulse energy to a level comparable with the pump pulse. In other words, generation of high-energy, wavelength tunable signal pulses constitutes the solution to achieve high power mid-IR frequency combs. Recently we demonstrated an energy-scalable fiber-optic technique in order to derive wavelength tunable signal pulses. We employ self-phase modulation (SPM) to broaden a narrow input optical spectrum to generate well-isolated spectral lobes and then spectrally filter the left-most/right-most spectral lobes to produce nearly transform-limited femtosecond pulses [35]. Based on a 30-MHz Yb:fiber laser system, such SPM-enabled spectral selection (SESS) approach is able to generate 100 fs pulses with up to 20 nJ pulse energy, tunable in the range of 1100-1200 nm [35]. Using these SESS pulses as the signal pulses, DFG inside 2-mm-thick GaSe can generate idler pulses in the wavelength range of 7–18 μm [14]. Our simulation results predict that DFG seeded by 10-nJ signal pulses and 100-nJ pump pulses can generate 0.13-nJ idler pulse from 2-mm-thick GaSe, corresponding to 3.9-mW output power at 30-MHz repetition rate. In [14], the measured mid-IR power under such launching condition is ~2.9-mW. Such power discrepancy may be due to the absence of multi-photon absorption and linear absorption in our modeling.

SESS exhibits excellent energy scalability and can be adapted to other laser wavelengths. For example, employing an ultrafast Er:fiber laser centered at 1.55 μm, we implemented a SESS source tunable from 1.3 μm to 1.7 μm with up to 16-nJ pulse energy [36]. We further showed that

Optics EXPRESS

such increasing the input pulse energy to ~1-μJ (offered by an OPA source) produced >100-nJ femtosecond pulses at 1.3 μm and 1.7 μm with a pulse peak power reaching the MW level.

We plan to implement such a SESS source based on a high power 2-μm laser system. The source laser under construction is a Tm-fiber laser at tens of MHz repetition rate and provides 2-μm femtosecond pulses with ~ μJ level pulse energy. Using proper fiber to implement SESS, signal pulses tunable in 2.2–2.9 μm with >100-nJ energy are possible and should enable generation of ~40 nJ mid-IR pulses tunable in 6–20 μm. We believe such a powerful source will open many new applications.

5. Conclusion

In conclusion, we numerically investigated HRR inter-pulse DFG, in which the crystal damage threshold limits the allowed pulse energy. We show that, different from OPAs based on low repetition-rate DFG, HRR DFG may operate in the linear regime, in which the idler pulse energy scales almost linearly with respect to the pump/signal pulse energy. Consequently increasing the signal energy is as efficient as increasing the pump energy for idler energy scaling in HRR DFG. We compare 1-μm driven DFG and 2-μm driven DFG, and demonstrate that 2-μm driven DFG has the following advantages:

1. The idler energy scalability benefits from smaller GVM, and therefore 2-μm driven DFG associated with a reduced GVM compared with the 1-μm driven case exhibits superior energy scalability for the idler pulses. More important, higher crystal damage threshold is expected due to the lower photon energy, and therefore more energetic pump pulses are allowed in the 2-μm driven DFG, which results in operation of inter-pulse DFG in the OPA regime.

2. The 2-μm driven DFG experiences a smaller dispersion and a larger phase matching bandwidth, which in conjunction with the reduced GVM results in much shorter idler pulses with close to be transform-limited pulse duration. Under the same launching conditions, the peak power of idler pulses generated in the 2-μm driven DFG is nearly two orders of magnitude higher than can be achieved from the 1-μm driven DFG (e.g., 72 kW versus 1.3 kW).

The key for achieving high power, HRR DFG is to obtain high energy (≥100 nJ) signal pulses. We show that SESS is a feasible approach to produce these required signal pulses. Ongoing work is to implement such HRR DFG experimentally and demonstrate its energy scalability. We anticipate that longwave mid-IR frequency combs with >2-W average power can be achieved by 2-μm driven inter-pulse DFG, which will open up avenues for many applications.

Funding

National Natural Science Foundation of China (11774234); Helmholtz Association (VH-NG-804); Helmholtz-CAS Joint Research Group (HCJRG 201); Deutsche Forschungsgemeinschaft (EXC 2056 - project ID 390715994).

References

1. H. Pires, M. Baudisch, D. Sanchez, M. Hemmer, and J. Biegert, "Ultrashort pulse generation in the mid-IR," Prog. Quantum Electron. **43**, 1–30 (2015).
2. A. Schliesser, N. Picqué, and T. W. Hänsch, "Mid-infrared frequency combs," Nat. Photonics **6**(7), 440–449 (2012).
3. F. Keilmann, C. Gohle, and R. Holzwarth, "Time-domain mid-infrared frequency-comb spectrometer," Opt. Lett. **29**(13), 1542–1544 (2004).
4. I. Coddington, N. Newbury, and W. Swann, "Dual-comb spectroscopy," Optica **3**(4), 414–426 (2016).
5. G. Ycas, F. R. Giorgetta, E. Baumann, I. Coddington, D. Herman, S. A. Diddams, and N. R. Newbury, "High-coherence mid-infrared dual-comb spectroscopy spanning 2.6 to 5.2 μm," Nat. Photonics **12**(4), 202–208 (2018).

Optics EXPRESS

6. H. Timmers, A. Kowligy, A. Lind, F. C. Cruz, N. Nader, M. Silfies, G. Ycas, T. K. Allison, P. G. Schunemann, S. B. Papp, and S. A. Diddams, "Molecular fingerprinting with bright, broadband infrared frequency combs," Optica **5**(6), 727–732 (2018).
7. B. Bernhardt, A. Ozawa, P. Jacquet, M. Jacquey, Y. Kobayashi, T. Udem, R. Holzwarth, G. Guelachvili, T. W. Hänsch, and N. Picqué, "Cavity-enhanced dual-comb spectroscopy," Nat. Photonics **4**(1), 55–57 (2010).
8. A. Foltynowicz, P. Masłowski, A. J. Fleisher, B. J. Bjork, and J. Ye, "Cavity-enhanced optical frequency comb spectroscopy in the mid-infrared application to trace detection of hydrogen peroxide," Appl. Phys. B **110**(2), 163–175 (2013).
9. R. Huber, A. Brodschelm, F. Tauser, and A. Leitenstorfer, "Generation and field-resolved detection of femtosecond electromagnetic pulses tunable up to 41 THz," Appl. Phys. Lett. **76**(22), 3191–3193 (2000).
10. F. Keilmann and S. Amarie, "Mid-infrared frequency comb spanning an octave based on an Er fiber laser and difference-frequency generation," J. Infrared, Millimeter, Terahertz Waves **33**(5), 479–484 (2012).
11. A. Ruehl, A. Gambetta, I. Hartl, M. E. Fermann, K. S. E. Eikema, and M. Marangoni, "Widely-tunable mid-infrared frequency comb source based on difference frequency generation," Opt. Lett. **37**(12), 2232–2234 (2012).
12. C. R. Phillips, J. Jiang, C. Mohr, A. C. Lin, C. Langrock, M. Snure, D. Bliss, M. Zhu, I. Hartl, J. S. Harris, M. E. Fermann, and M. M. Fejer, "Widely tunable midinfrared difference frequency generation in orientation-patterned GaAs pumped with a femtosecond Tm-fiber system," Opt. Lett. **37**(14), 2928–2930 (2012).
13. A. Gambetta, N. Coluccelli, M. Cassinerio, D. Gatti, P. Laporta, G. Galzerano, and M. Marangoni, "Milliwatt-level frequency combs in the 8–14 μm range via difference frequency generation from an Er:fiber oscillator," Opt. Lett. **38**(7), 1155–1157 (2013).
14. G. Zhou, Q. Cao, F. X. Kärtner, and G. Chang, "Energy scalable, offset-free ultrafast mid-infrared source harnessing self-phase-modulation-enabled spectral selection," Opt. Lett. **43**(12), 2953–2956 (2018).
15. A. Baltuška, T. Fuji, and T. Kobayashi, "Controlling the carrier-envelope phase of ultrashort light pulses with optical parametric amplifiers," Phys. Rev. Lett. **88**(13), 133901 (2002).
16. I. Pupeza, D. Sánchez, J. Zhang, N. Lilienfein, M. Seidel, N. Karpowicz, T. Paasch-Colberg, I. Znakovskaya, M. Pescher, W. Schweinberger, V. Pervak, E. Fill, O. Pronin, Z. Wei, F. Krausz, A. Apolonski, and J. Biegert, "High-power sub-two-cycle mid-infrared pulses at 100 MHz repetition rate," Nat. Photonics **9**(11), 721–724 (2015).
17. L. Maidment, P. G. Schunemann, and D. T. Reid, "Molecular fingerprint-region spectroscopy from 5 to 12 μm using an orientation-patterned gallium phosphide optical parametric oscillator," Opt. Lett. **41**(18), 4261–4264 (2016).
18. K. Iwakuni, G. Porat, T. Q. Bui, B. J. Bjork, S. B. Schoun, O. H. Heckl, M. E. Fermann, and J. Ye, "Phase-stabilized 100 mW frequency comb near 10 μm," Appl. Phys. B **124**(7), 128 (2018).
19. D. Sanchez, M. Hemmer, M. Baudisch, S. L. Cousin, K. Zawilski, P. Schunemann, O. Chalus, C. Simon-Boisson, and J. Biegert, "7 μm, ultrafast, sub-millijoule-level mid-infrared optical parametric chirped pulse amplifier pumped at 2 μm," Optica **3**(2), 147–150 (2016).
20. R. Hegenbarth, A. Steinmann, S. Sarkisov, and H. Giessen, "Milliwatt-level mid-infrared (10.5–16.5 μm) difference frequency generation with a femtosecond dual-signal-wavelength optical parametric oscillator," Opt. Lett. **37**(17), 3513–3515 (2012).
21. J. Zhang, K. F. Mak, N. Nagl, M. Seidel, D. Bauer, D. Sutter, V. Pervak, F. Krausz, and O. Pronin, "Multi-mW, few-cycle mid-infrared continuum spanning from 500 to 2250 cm^{-1}," Light: Sci. Appl. **7**(2), 17180 (2018).
22. C. Gaida, M. Gebhardt, T. Heuermann, F. Stutzki, C. Jauregui, J. Antonio-Lopez, A. Schülzgen, R. Amezcua-Correa, A. Tünnermann, I. Pupeza, and J. Limpert, "Watt-scale super-octave mid-infrared intrapulse difference frequency generation," Light: Sci. Appl. **7**(1), 94 (2018).
23. T. P. Butler, D. Gerz, C. Hofer, J. Xu, C. Gaida, T. Heuermann, M. Gebhardt, L. Vamos, W. Schweinberger, J. A. Gessner, T. Siefke, M. Heusinger, U. Zeitner, A. Apolonski, N. Karpowicz, J. Limpert, F. Krausz, and I. Pupeza, "Watt-scale 50-MHz source of single-cycle waveform-stable pulses in the molecular fingerprint region," Opt. Lett. **44**(7), 1730–1733 (2019).
24. S. Vasilyev, I. S. Moskalev, V. O. Smolski, J. M. Peppers, M. Mirov, A. V. Muraviev, K. Zawilski, P. G. Schunemann, S. B. Mirov, K. L. Vodopyanov, and V. P. Gapontsev, "Super-octave longwave mid-infrared coherent transients produced by optical rectification of few-cycle 2.5-μm pulses," Optica **6**(1), 111–114 (2019).
25. Q. Wang, J. Zhang, A. Kessel, N. Nagl, V. Pervak, O. Pronin, and K. F. Mak, "Broadband mid-infrared coverage (2–17 μm) with few-cycle pulses via cascaded parametric processes," Opt. Lett. **44**(10), 2566–2569 (2019).
26. D. Sanchez, M. Hemmer, M. Baudisch, K. Zawilski, P. Schunemann, H. Hoogland, R. Holzwarth, and J. Biegert, "Broadband mid-ir frequency comb with $CdSiP_2$ and $AgGaS_2$ from an Er,Tm:Ho fiber laser," Opt. Lett. **39**(24), 6883–6886 (2014).
27. K. S. Abedin, S. Haidar, Y. Konno, C. Takyu, and H. Ito, "Difference frequency generation of 5–18 μm in a $AgGaSe_2$ crystal," Appl. Opt. **37**(9), 1642–1646 (1998).
28. M. Beutler, I. Rimke, E. Büttner, P. Farinello, A. Agnesi, V. Badikov, D. Badikov, and V. Petrov, "Difference-frequency generation of ultrashort pulses in the mid-IR using Yb-fiber pump systems and $AgGaSe_2$," Opt. Express **23**(3), 2730–2736 (2015).
29. T. Steinle, F. Mörz, A. Steinmann, and H. Giessen, "Ultra-stable high average power femtosecond laser system tunable from 1.33 to 20 μm," Opt. Lett. **41**(21), 4863–4866 (2016).
30. K. L. Vodopyanov and P. G. Schunemann, "Broadly tunable noncritically phase-matched $ZnGeP_2$ optical parametric oscillator with a 2-μJ pump threshold," Opt. Lett. **28**(6), 441–443 (2003).

Optics EXPRESS

31. A. Dergachev, D. Armstrong, A. Smith, T. Drake, and M. Dubois, "3.4-μm ZGP RISTRA nanosecond optical parametric oscillator pumped by a 2.05-μm Ho:YLF MOPA system," Opt. Express **15**(22), 14404–14413 (2007).
32. P. E. Powers and J. W. Haus, *Fundamentals of nonlinear optics* (CRC press, 2017).
33. J. A. Armstrong, N. Bloembergen, J. Ducuing, and P. S. Pershan, "Interactions between light waves in a nonlinear dielectric," Phys. Rev. **127**(6), 1918–1939 (1962).
34. K. Liu, H. Liang, L. Wang, S. Qu, T. Lang, H. Li, Q. J. Wang, and Y. Zhang, "Multimicrojoule GaSe-based midinfrared optical parametric amplifier with an ultrabroad idler spectrum covering 4.2–16 μm," Opt. Lett. **44**(4), 1003–1006 (2019).
35. W. Liu, C. Li, Z. Zhang, F. X. Kärtner, and G. Chang, "Self-phase modulation enabled, wavelength-tunable ultrafast fiber laser sources: an energy scalable approach," Opt. Express **24**(14), 15328–15340 (2016).
36. H.-Y. Chung, W. Liu, Q. Cao, L. Song, F. X. Kärtner, and G. Chang, "Megawatt peak power tunable femtosecond source based on self-phase modulation enabled spectral selection," Opt. Express **26**(3), 3684–3695 (2018).